European Union
European Social Fund
OPERATIONAL PROGRAMME
EDUCATION AND LIFELONG LEARNING
investing in knowledge society
MINISTRY OF EDUCATION & RELIGIOUS AFFAIRS, CULTURE & SPORTS
MANAGING AUTHORITY
NSRF 2007-2013
programme for development
EUROPEAN SOCIAL FUND
Co-financed by Greece and the European Union

Behavior of very tall concrete faced rockfill dams during impoundment

E. Stavrotheodorou
Department of Civil Engineering
University of Thessaly
Pedion Areos
Volos, 38334
Greece

P. Dakoulas
Department of Civil Engineering
University of Thessaly
Pedion Areos
Volos, 38334
Greece

Introduction

This paper investigates the behavior of three tall concrete faced rockfill dams (CFRDs), of height equal to 100 m, 200 m and 300 m, respectively. The study is based on a nonlinear 3-D numerical simulation of the phased construction of each dam and subsequent reservoir impoundment. Emphasis is placed on the effect of rockfill stiffness and dam height on the development of (a) rockfill settlements and (b) high compressive stresses in the slab after impoundment. The analysis is based on a robust finite element formulation using the nonlinear Duncan and Chang model for rockfill and gravel. The slab behavior is modeled using the concrete damaged plasticity model by Lee and Fenves [8], which takes into account the effects of strain softening and accumulated damage due to cracking, distinguishing between the damage variables for tension and compression. This model incorporates a degradation mechanism that represents the effects of damage on the elastic stiffness and the recovery of stiffness after crack closure. To significantly increase the ductility, a fiber-reinforced concrete is considered for the three face slabs. The three dams are built in narrow canyons having an aspect ratio equal to L/H=2. The upstream slope is 1:1.4, whereas the downstream slope is 1:1.5. The main material zones considered for the numerical analysis are the upstream zone 3B, the downstream zone 3C and a gravel zone 2B beneath the slab. The embankment construction for the three dams is simulated using 40 height lifts. The material parameters for the rockfill model are calibrated based on the actual measurements of settlements in the middle section from existing dams of similar heights (for H = 100 m and 200 m). The upstream slab consists of 14, 28 and 40 independent concrete panels, respectively, for the three dams. Each panel has steel rebar reinforcement in two directions. Furthermore, each panel has proper frictional conditions and gap opening capability at its base interface with the gravel layer and at its vertical interface with the neighboring panels. The combined effects of rockfill settlements due to reservoir impoundment and creep, as well as potential seismic movements and dynamic rockfill settlements, may cause high compressive stresses in the vertical walls of adjacent concrete panels, especially in the middle part of the concrete slab. This study focuses mainly on the magnitude of tensile stress damage developing in the concrete slab after impoundment and the compressive stresses caused by the combined effect of impoundment, creep and dynamic settlements.

1. Performance of extra-high concrete faced rockfill dams

The number of concrete faced rockfill dams continues to increase worldwide, due to their significant advantages, such as their adaptability to topographical and geological conditions and to rainy or even harsh climate, the smaller volume of construction materials, the smaller demand for materials from distant regions, the faster construction process, safer operation and easier maintenance [1].

The general experience from the performance of tall CFRDs shows that during impoundment tensile cracks may develop along the perimeter of the slab [3]. Moreover, use of poor rockfill material or inadequate compaction may cause significant rockfill settlements, which may lead to compressive stresses and spalling of the concrete panels [1,3]. Water leakage may further increase settlements due to washing out of the finer materials and cause additional cracking and spalling in the slab. Finally, in dams built in earthquake regions, seismic transient stresses and stresses caused by accumulated dynamic settlements may significantly increase compression along the walls of the vertical joints causing spalling [4,6,7].

To respond to the increasing need for water and clean energy production, extra-high CFRDs, having a height > 150 m, are currently designed and built in various parts of the world. Such an example is the Shuibuya concrete faced rockfill dam, completed in 2007 in China, having a height of 233 m. Moreover, new dams of height reaching the level of 300 m are currently under design. Since there is very little experience regarding the performance of CFRDs with height > 200 m, it is of interest to investigate numerically the effect of dam height on the performance of concrete slab, and make comparisons with observed performance of smaller-height existing dams.

2. Numerical modelling

2.1 Dam geometry

Fig. 1 illustrates the geometry and material zones of all three dams considered. They are built in narrow canyons, having a trapezoidal shape with the same aspect ratio equal to L/H=2. The upstream slope is 1:1.4, whereas the downstream slope is 1:1.5. The main material zones considered for the numerical analysis are the upstream zone 3B, the downstream zone 3C and a gravel zone 2B beneath the slab. The upstream slab consists of 14, 28 and 40 independent concrete panels, respectively, for the three dams. The slab panels have a width of 15 m and thickness given by $t = 0.30 + 0.003h$, where h is the height of the overlying water. Each panel has steel rebar reinforcement in two directions. Furthermore, each panel has proper frictional conditions and gap opening capability at its base interface with the gravel layer and at its vertical interface with the neighboring panels.

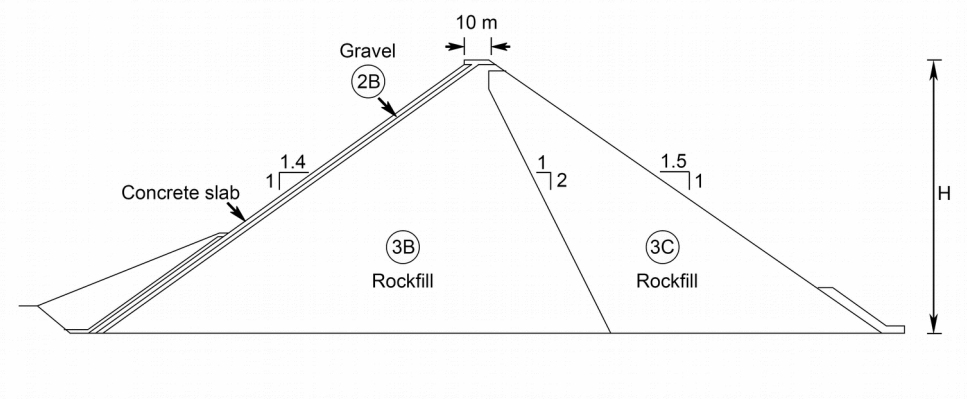

Fig 1. Dam cross-section and material zones of the three dams (H=100m, 200m, and 300m)

2.2 Numerical discretization

The structural integrity and watertightness of the face slab panels are of crucial importance with respect to the safety and good performance of the dam. In the case of dams built in narrow canyons, a realistic modeling of the 3D geometry of the slab panels, the nonlinear material behaviour and the contact conditions at the concrete base and the vertical joints between adjacent slab panels is essential. Ignoring the 3D nature of the problem or the presence of the vertical joints would result into predictions that do not capture the real behaviour of slab.

The numerical analysis is conducted using the general purpose finite element code ABAQUS [2]. Fig. 2 illustrates the numerical discretization of the three dams. Only half of the dam body is discretized taking advantage of its symmetry with respect to the mid-section. The embankment cross section is divided in 3 main zones: (a) the rockfill zone 3B, (b) the rockfill zone 3C and (c) the gravel zone 2B. The embankment body is divided in 40 layers in order to simulate the staged construction process. The finite element model of the embankment consists of 8-node, reduced integration hexahedral solid elements (C3D8-R). The slab panels are discretized using two layers of hexahedral solid elements (C3D8). The concrete behavior is modeled using the damage plasticity model discussed in

Section 2.4 below. Reinforcement is placed at the mid-thickness of the slab, consisting of 25 mm diameter steel bars at 20 cm distance in the x and y directions of the concrete panels. Each panel has interface properties between its base and the underlying gravel, as well as between the vertical walls of adjacent slabs. The concrete-to-gravel friction coefficient is μ =0.8 and the concrete-to-concrete friction coefficient is μ_c =0.5.

2.3 Constitutive models for gravel and rockfill

Although the use of an elastoplastic model with hardening, stress-dependent elastic moduli and proper hysteretic behavior would simulate better the behavior of rockfill, the significant complexity of such a model and the lack of laboratory data for rockfill would be a serious disadvantage. The hypoelastic model by Duncan and Chang [9,10] has been used extensively for the modeling of the stress-strain behavior of rockfill in embankment dams [5,6,7]. The model uses a hyperbolic stress-strain relationship and accounts for the dependency of the elastic moduli on the current stress state and the loading/unloading stress path. The tangent Young's modulus given by:

$$E_t = K\ p_a \left(\frac{\sigma_3}{p_a} \right)^n \left| 1 - \frac{R_f (\sigma_1 - \sigma_3)(1 - \sin\phi)}{2\sigma_3 \sin\phi + 2c\cos\phi} \right|^2 \qquad (1)$$

where σ_1, σ_3 = principal stresses, K , R_f , n =material constants, φ =friction angle, c =cohesion, p_a =atmospheric pressure. The friction angle depends on the confining stress as follows $\phi = \phi_o - \Delta\phi \log(\sigma_3 / p_a)$ where ϕ_o and $\Delta\phi$ = material constants. The unloading modulus is given by

$$E_{ur} = K_{ur}\ p_a \left(\sigma_3 / p_a \right)^n \qquad (2)$$

where K_{ur} =material constant with a range of variation between $1.2K \le K_{ur} \le 3K$. The bulk modulus is given by

$$B = K_b\ p_a \left(\sigma_3 / p_a \right)^m \qquad (3)$$

where K_b , m =material constants. The main advantage of the model is the considerable accumulated experience regarding the model parameters for various types of rockfill materials [10], for which laboratory testing is difficult. Table 1 provides the properties and model constants for rockfill and gravel, used for the analysis of the three dams.

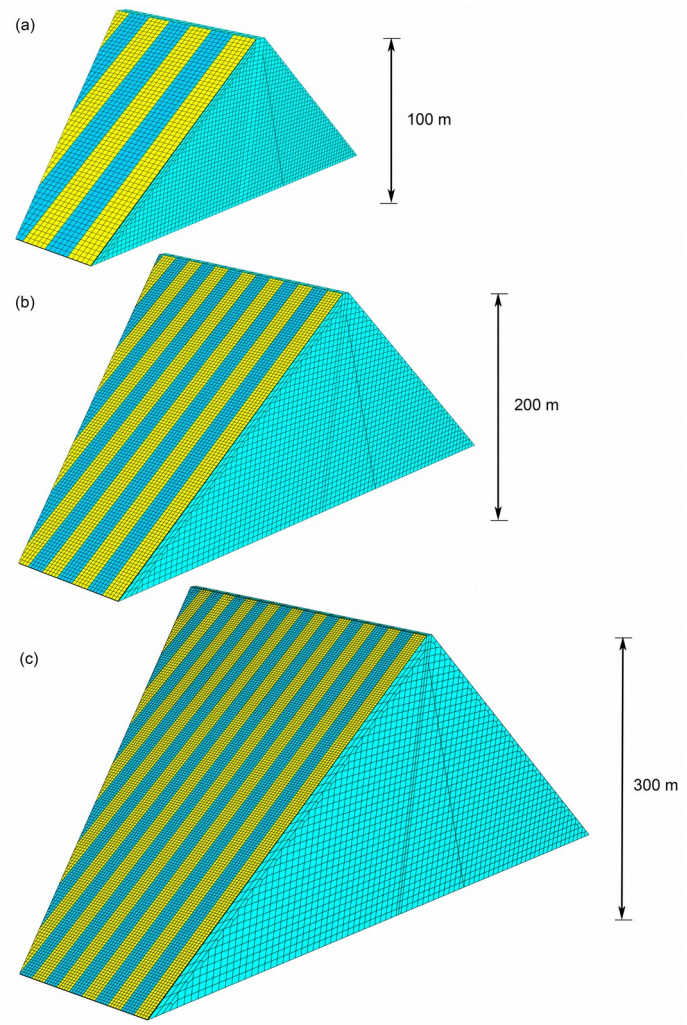

Fig 2. Finite element discretization of dam and slab geometry (a) 100m-high dam (b) 200m-high dam and (c) 300m-high dam

Table 1. Properties and model constants for rockfill and gravel zones of the three dams

	H = 100 m			**H = 200 m**			**H = 300 m**		
	3B	**2B**	**3C**	**3B**	**2B**	**3C**	**3B**	**2B**	**3C**
Density, ρ kg/m^3	2150	2150	2150	2150	2150	2150	2150	2150	2150
K	502	1004	377	805	1610	604	1036	2072	777
K_{ur}	1255	2510	942	2012	4025	1510	2590	5180	1942
K_b	125	251	94	201	402	151	259	518	194
n	0.45	0.45	0.45	0.45	0.45	0.45	0.45	0.45	0.45
m	0.22	0.22	0.22	0.22	0.22	0.22	0.22	0.22	0.22
R_f	0.59	0.59	0.59	0.59	0.59	0.59	0.59	0.59	0.59
ϕ_0	51°	51°	51°	51°	51°	51°	51°	51°	51°
$\Delta\phi$	9°	9°	9°	9°	9°	9°	9°	9°	9°

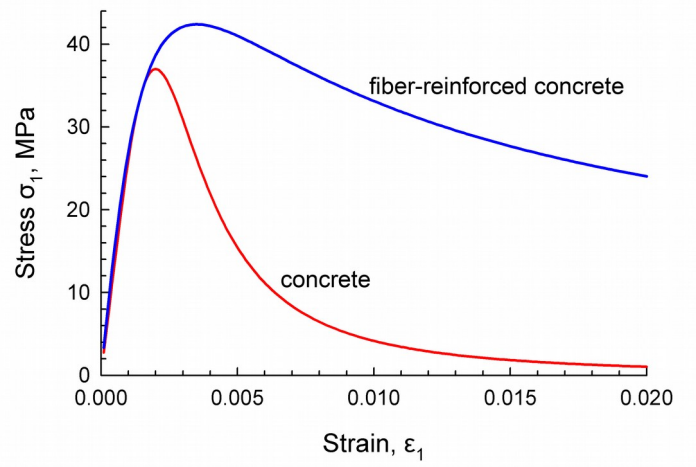

Fig 3. Comparison of the stress-strain behaviour of fiber-reinforced concrete and plain concrete using cubic specimens subjected to uniaxial compression based on Natarajia et al [11]

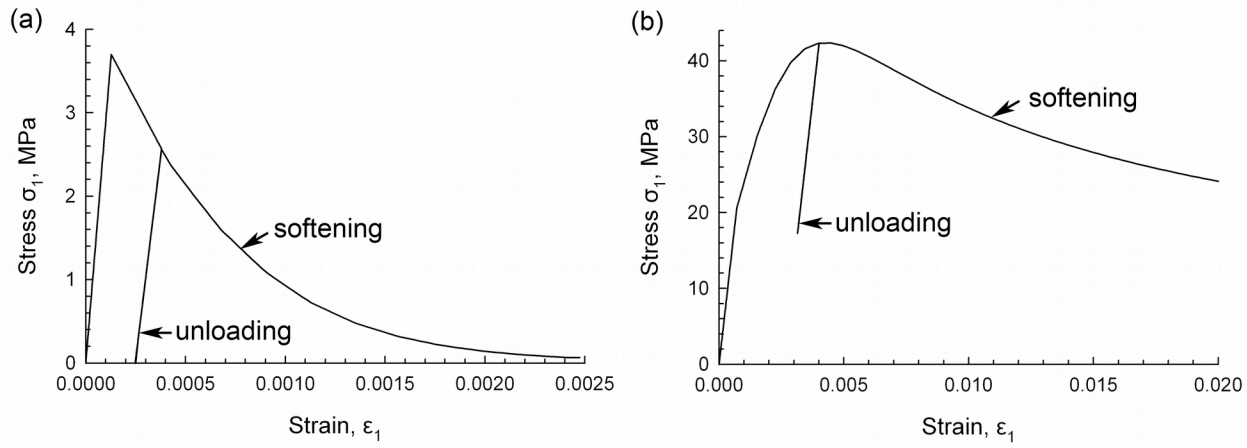

Fig 4. Stress-strain behaviour of fiber-reinforced concrete obtained from numerical simulations of (a) a uniaxial tension test and (b) a uniaxial compression test, with unloading and reloading segments, on cubic specimens (RI=2.5%)

2.4 Constitutive models for concrete

The damage plasticity constitutive model for cyclic loading of concrete developed by Lee and Fenves [8] is used here for modeling the behavior of the reinforced concrete panels. This rate-independent model takes into account the effects of strain softening, distinguishing between the damage variables for tension and compression. The model incorporates a degradation mechanism that represents the effects of damage on the elastic stiffness and the recovery of stiffness after crack closure. Details about the damage plasticity constitutive model, as well as comparisons of experimental data and simulations of the stress-strain behavior of concrete in cyclic tension and compression tests have been presented in [8].

It is of interest to improve concrete behavior for the extra-high concrete faced rockfill dams, by increasing its strength and ductility in order to accommodate larger tensile strains without significant cracking and larger compressive strains without spalling. To this end, the addition of steel-fibers significantly improves many of the engineering properties of mortar and concrete, such as: impact strength and toughness, flexural strength, fatigue strength, tensile strength and the ability to resist cracking and spalling [11]. The stress-strain relationship of the fiber-reinforced concrete depends on the compressive strength of the concrete used and the Reinforcing Index $RI = w_f l / d$, where w_f = weight fraction, l = length and d = diameter of the fiber. Fig. 3 plots the stress-strain behaviour of a cubic element of steel-fiber reinforced concrete and plain concrete in uniaxial compression based on extensive experimental data and analytical expressions by Natarajia et al [11]. The plain concrete used in both elements has a compressive strength of 37 MPa, whereas the fiber-reinforced concrete has a reinforcing index RI =

2.5%. It is evident in Fig. 3 that the fiber-reinforced concrete has a substantially higher ductility compared to the plain concrete and therefore it can accommodate better large compressive strains that may occur in the slab due to significant settlement. This high ductility is also present in the case of a tensile uniaxial test. In addition to steel fiber reinforcement, glass fiber and polypropylene fiber may also be used. For the upstream face concrete slab, the latter may have three significant additional advantages: higher ductility, higher hysteretic damping and no corrosion risk.

In the following analysis the concrete slab in all dams is assumed to have a density ρ =2350, kg/m^3, fiber-reinforced concrete compressive strength of 42.4 MPa, tensile strength of 3.7 MPa, elastic Young's modulus E = 29 GPa and Poisson's ratio ν = 0.2. This fiber-reinforced concrete is assumed to be made up by mixing plain concrete of compressive strength of 37 MPa and fiber corresponding to a reinforcing index RI = 2.5%. Figure 4 plots numerical simulations of the stress-strain behavior of two cubic concrete specimens in uniaxial loading using the damage plasticity model. For the tension test in Fig. 4a, the effect of the accumulated damage representing tensile cracks is taken into account, whereas for the compression test in Fig. 4b, it is ignored in the present study.

3. Simulation of phased construction and impoundment

3.1 Rockfill settlements

The simulation of the staged construction is performed in forty increments. The material parameters K , K_{ur} and K_b in equations (1)-(3) are calibrated through iterations, assuming that the anticipated maximum staged-construction settlement S_{max} will be equal to 1.5% of the dam height. Thus, for the three dams investigated, the computed settlements are exactly equal to 1.5 m, 3 m and 4.5 m, respectively. Fig. 5 plots the distribution of the computed settlements at the middle cross-section at the end of the staged construction.

It should be noted that the stiffness parameters K in equation (1) increase with the dam height in order to maintain a constant ratio $S_{\max} / H$ =0.015. Thus, for H =100 m, 200 m, and 300 m, the corresponding values of K are 502, 805 and 1036, respectively. Assuming that the nonlinear dependency of E , E_{ur} and B on the stress level expressed in equations (1)-(3) is valid for the entire range of stresses developing in the three dams, this implies that the quality of compaction must increase with the dam height in order to maintain the desirable performance of the slab.

3.2 Slab deflection and movement after impoundment

After completion of the embankment, the concrete slab panels are placed on the upstream slope surface. The upstream surface node coordinates are modified through a single iteration so that after completion of the construction settlements the surface remains a perfect plane, without imposing any initial (artificial) deformation on the slab. Support along the perimeter of the slab simulates the support by the plinth.

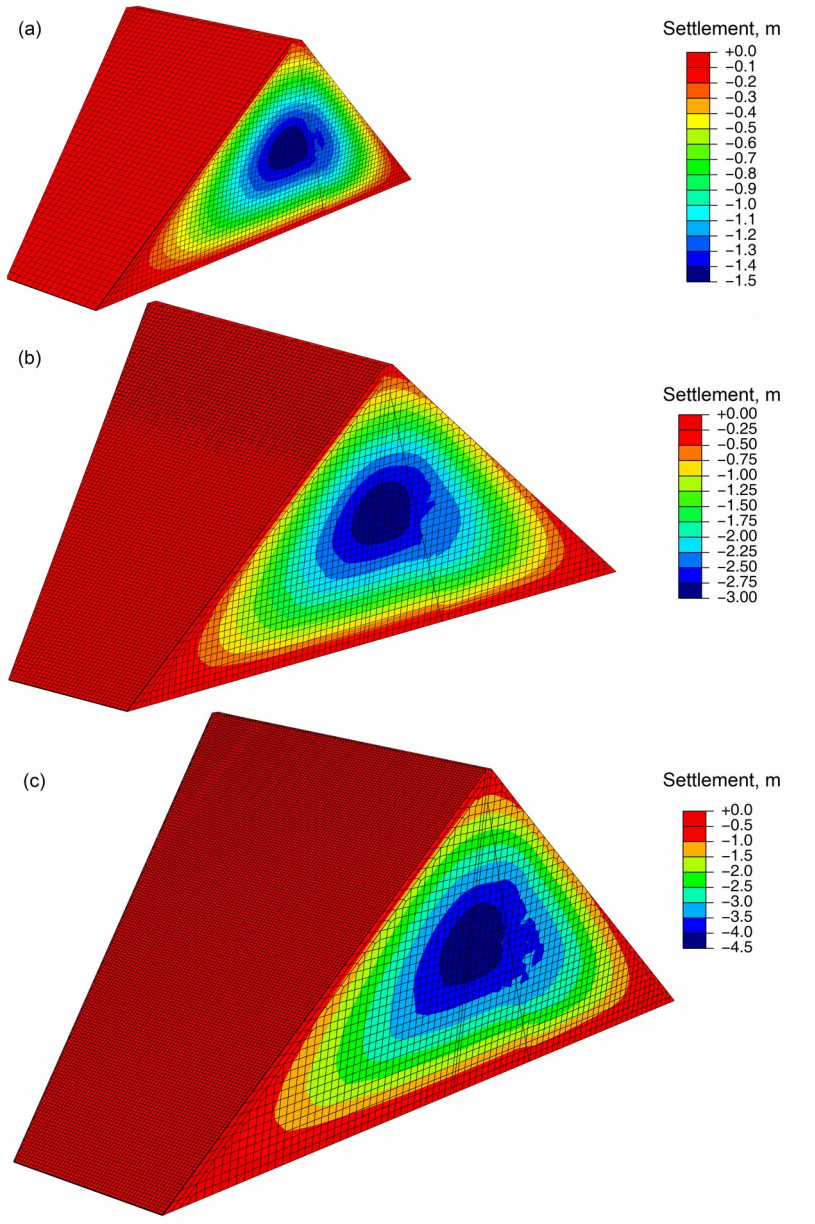

Fig 5. Construction settlements (a) 100m-high dam (b) 200m-high dam and (c) 300m-high dam

In typical CFRD designs, a fill is placed on the lower part of the slab, as shown Fig. 1. Such a fill has not been incorporated in this analysis, but it can be added in a straightforward manner later on.

Finally, the reservoir water is raised gradually from lower levels to the maximum levels, which correspond to 98 m, 198 m and 298 m, respectively, for the three dams. Fig. 6 plots the deflection U_z of the three slabs, measured in the direction normal to its surface, after impoundment. For the 100 m dam, the maximum value of the slab deflection is 32.5 cm, for the 200 m dam it is 46 cm and for the 300 m it is 59 cm. Considering the substantial increase of height from 100 m to 300 m, the deflection of the tallest dam is within reasonable limits. In all three dams, the maximum value of slab deflection occurs at midsection at a height equal to about $H/3$.

During impoundment, due to the deformation of the underlying rockfill and the high friction at the slab base, the slab panels tend to move towards the crest and the middle section of the dam, with a maximum displacement. Thus, for the three dams, the maximum panel movement in the x direction near the toe is only about 3.5cm. Similarly, the maximum panel movement in the y direction has a value of only about 4 cm. Hence, the opening of the joints is less than the typical 10 cm limit of the waterstops along the plinth and the vertical joints.

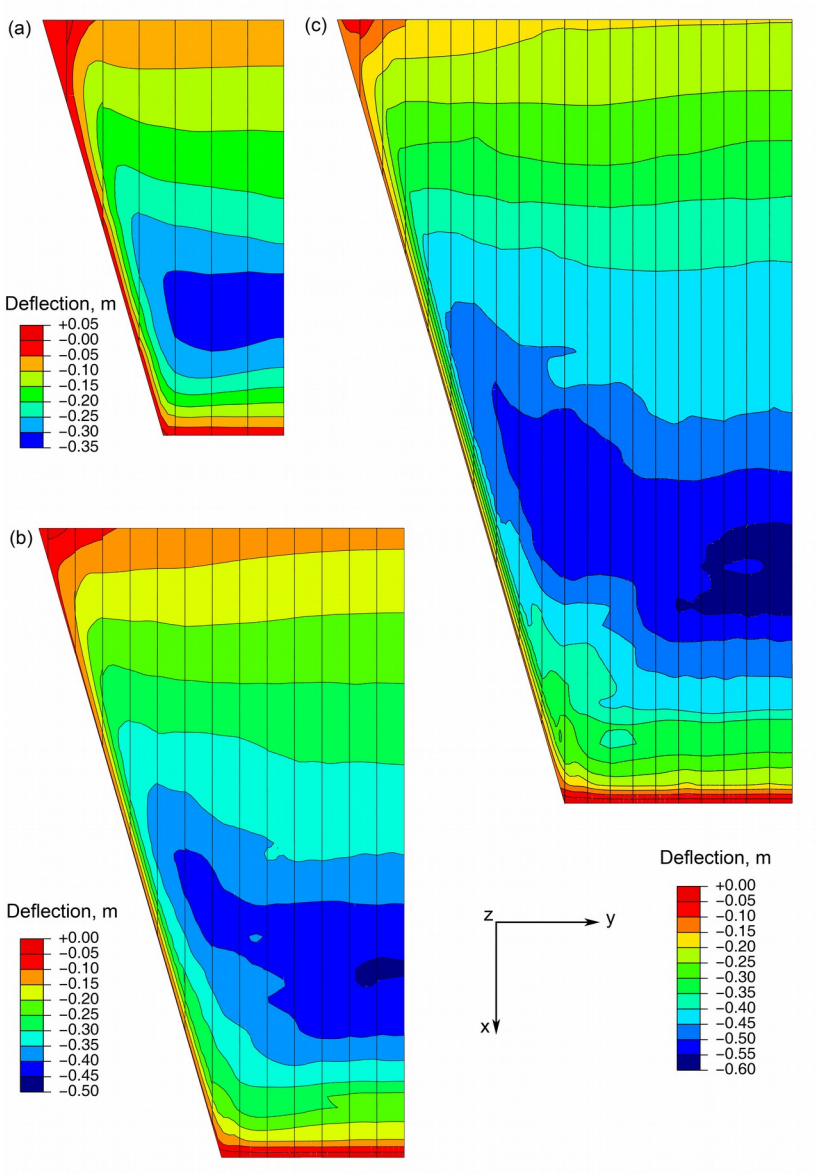

Fig 6. Contours of slab deflection after impoundment (a) 100m-high dam (b) 200m-high dam and (c) 300m-high dam

3.3 Slab tensile stress damage and maximum compression

Fig. 7 plots the distribution of damage factor at the *top surface* of the slab due to tensile stresses exceeding the elastic limit (Fig. 4a). After yielding, a significant softening of the material develops, as shown in Fig. 4a, with simultaneous development of tensile cracks. Therefore, in this case it is more useful to examine the damage factor in tension than the actual magnitude to the major principal stress σ_1. Zero damage means that the stresses did not exceed the elastic limit, whereas damage equal to one implies maximum tensile cracking of the concrete.

For the smaller 100m-high dam, it is evident that there is very little or negligible damage of the slab due to tensile stresses. For the 200m-dam, however, there is significant tensile damage developing near the left abutment and at the toe of the slab panels. Even higher damage occurs in the case of the 300 m dam, appearing at the same location as in the case of the 200 m dam. Such tensile stresses develop due to a significant variation of the underlying rockfill stiffness from the slab toe towards the crest. Tensile cracks may develop in these regions, so they must be protected with a proper fill or other means against water leakage.

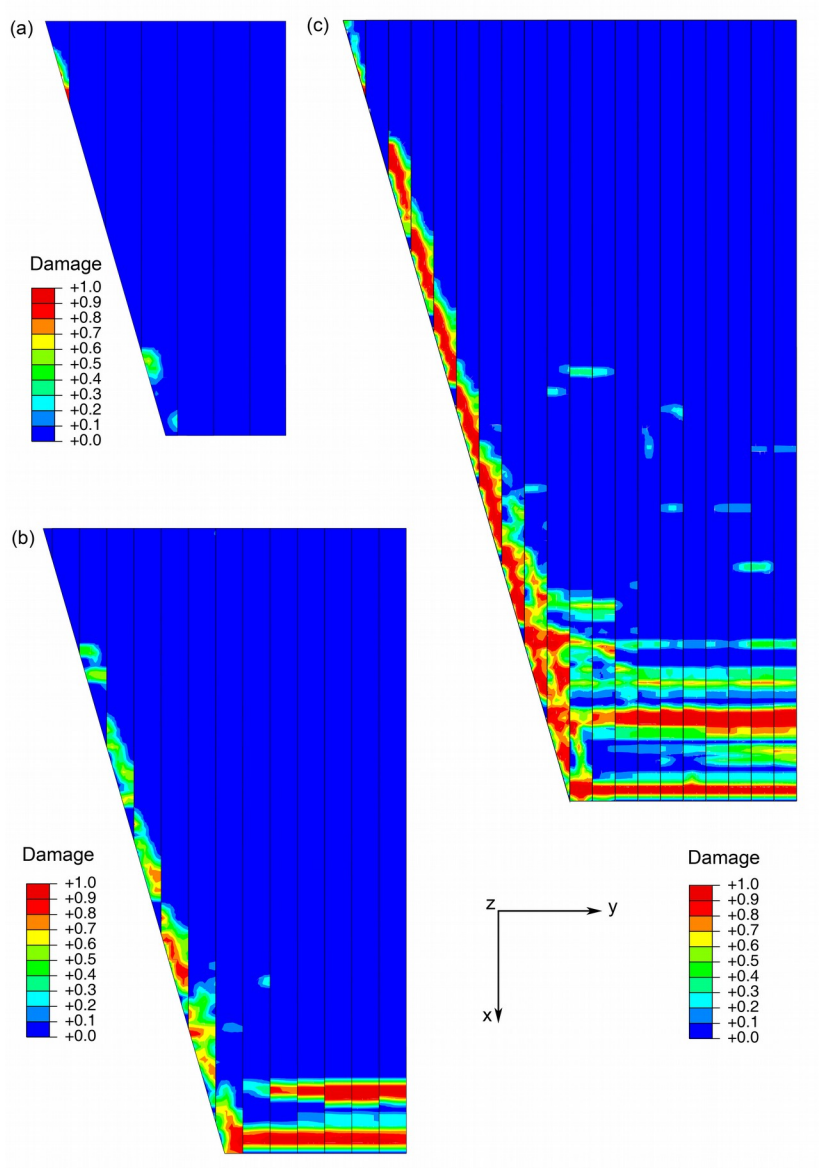

Fig 7. Contours of tensile damage factor after impoundment (a) 100m-high dam (b) 200m-high dam and (c) 300m-high dam

The tensile damage bands that appear at the toe of the central region may be explained by the softening material behavior, resulting to localization of tensile strain or cracking (as in the case of shear banding). The presence of a tensile zone that is parallel to the perimetric plinth, as that in Fig. 7, is in agreement with the reported 10 to 20 m-wide zone of cracking in existing dams, such as Xingó, Itá and Itapebi [3]. It should be noted that, in the case of additional creep or dynamic settlements, tensile stresses tend to reduce, as the rockfill settlement pushes the panels towards the toe plinth, through the high frictional forces at the base interface. Thus the critical stage for tensile stresses is during impoundment. By contrast, the maximum compression due to impoundment (not shown here) is not significant. The maximum compressive stress occurs at the toe region of the slab panels near the abutment and is equal to about -10 MPa for all three dams (compression has negative values).

In order to simulate approximately the effects of the anticipated creep and dynamic settlements, the gravity load on the dam body is increased artificially and decreased again to the previous value, yielding a net settlement equal to the estimated value, based on previous experience. Thus, after impoundment, an additional combined creep and dynamic settlements equal to S/H =0.5% is imposed on the rockfill for each dam.

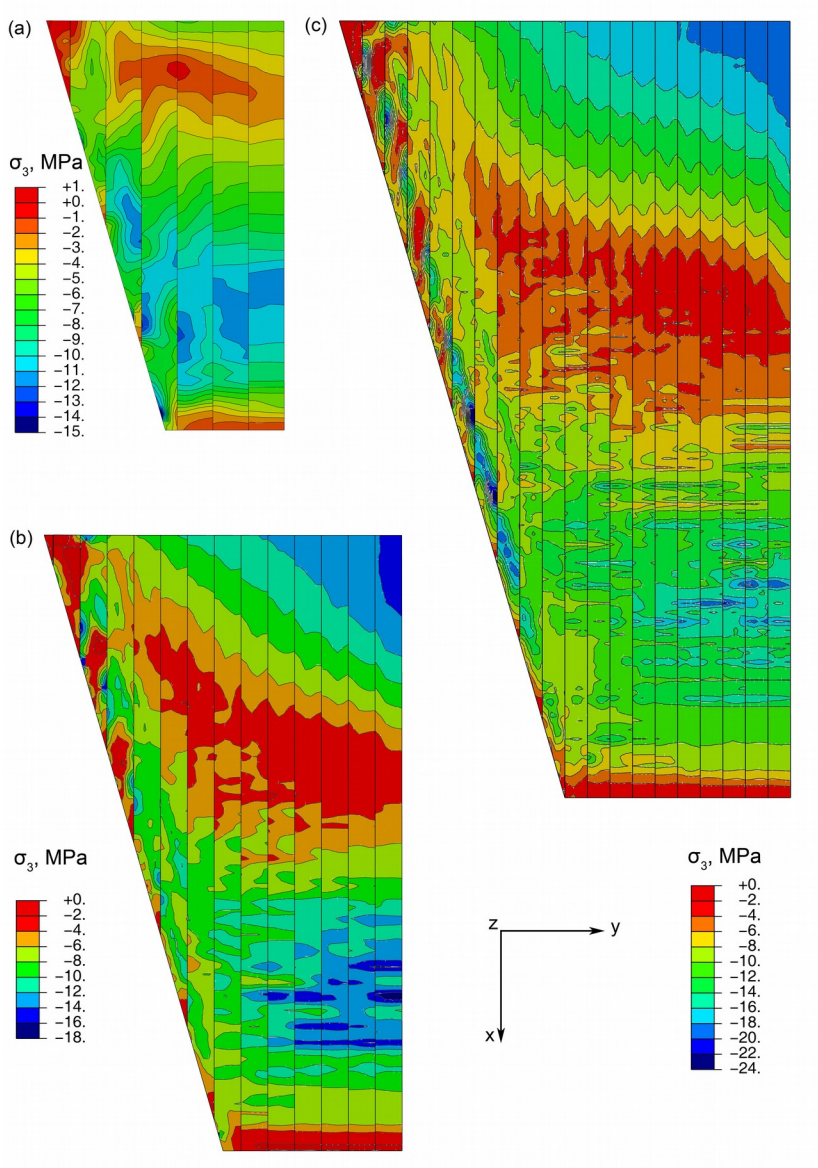

Fig 8. Contours of minimum principal stress (maximum compression) after application of impoundment load, creep and dynamic settlement (a) 100m-high dam (b) 200m-high dam and (c) 300m-high dam

Fig. 8 plots contours of the minor principal stress σ_3, indicating maximum compression, at the *top surface* of the slab. The maximum values of compressive stress are about 15 MPa, 18 MPa and 24 MPa for the three dams, respectively. It is noted that these maximum values are well below the compressive strength of the fiber-reinforced concrete (42.4 MPa), allowing a considerable margin of safety that most likely would be adequate in the case of additional compressive stresses, such as from a very strong ground shaking.

4. Conclusions

This paper investigated the behavior of three tall concrete faced rockfill dams (CFRDs), having a height equal to 100 m, 200 m and 300 m, respectively. The study was based on a nonlinear 3-D numerical simulation of the phased construction of each dam, reservoir impoundment and subsequent creep and dynamic settlements. The slab consists of a fiber-reinforced concrete that allows a much higher ductility, which is very desirable in the case of the extra-high dams. The behavior of the fiber-reinforced concrete is modeled using the damaged plasticity model by Lee and Fenves [8]. Emphasis is placed on the slab performance of the 200m- and 300m-high dams.

The main conclusions of the study are the following:

1. As the dam height increases, in order to limit the ratio of construction settlement S_{max}/H to a desirable value (e.g. <1.5%) that will allow a good performance of the slab, the quality of rockfill compaction must increase.
2. For a construction settlement ratio of S_{max}/H =1.5%, the computed slab defections after impoundment are limited within acceptable values.
3. For the 200m- and 300m-dams, the accumulated damage during impoundment due to tensile stresses near the abutment and the lower region of the slab panels seems significant and therefore cracking may occur in these regions. To prevent water leakage, these areas should be properly protected with a fill cover or other means.
4. Maximum compressive stresses after impoundment are less than ¼ of the compressive strength of the fiber-reinforced concrete for all dams.
5. For the 300m-high dam, maximum compressive stresses in the slab after additional combined creep and dynamic settlements equal to S/H =0.5% are less than 24 MPa, i.e. well below the compressive strength.
6. The overall performance of all three dams seems to be satisfactory, allowing adequate margins of safety.

5. Acknowledgements

This research has been co-financed by the European Union (European Social Fund – ESF) and Greek national funds through the Operational Program "Education and Lifelong Learning" of the National Strategic Reference Framework (NSRF)-Research Funding Program: Heracleitus II. Investing in knowledge society through the European Social Fund.

References

1. **Ma, H.** and CAO, K., "Key technical problems of extra-high concrete faced rockfill dam" *Science in China, Series E, Technological Sciences*, 2007,50, 20-33
2. **ABAQUS,** Users' Manual, Simulia, Pawtucket, Rhode Island, 2011.
3. **Marques Filho, F., Pinto N.,** "CFRD dam characteristics learned from experience", *Hydropower & Dams*, 2005; 1:72-76
4. **Guan, Z.,** "Investigation of the 5.12 Wenchuan Earthquake damages to Zipingpu Water Control Project and an assessment of its safety state", *Science in China*, *Series E, Technological Sciences*, 2009; 52(4):820-834.
5. **Dakoulas, P., Thanopoulos, Y., and Anastassopoulos, K.**, "Nonlinear 3D simulation of CFR dam construction and reservoir filling", International Journal of Hydropower and Dams, 2008, Issue 2, 95-101.
6. **Dakoulas, P.**, "Nonlinear seismic response of tall concrete faced rockfill dams in narrow canyons" *Soil Dynamics and Earthquake Engineering*, 2012, 34, 11-24.
7. **Dakoulas, P.**, "Longitudinal vibrations of tall concrete faced rockfill dams in narrow canyons", *Soil Dynamics and Earthquake Engineering*, 2012, 41, 44-58.
8. **Lee J., Fenves, G.L,** "A plastic-damage concrete model for earthquake analysis of dams", Journal of Earthq. Eng. & Struct. Dynamics 1998; 27: 937-596.
9. **Duncan J. M., Chang C. Y.,** "Nonlinear analysis of stress and strain in soils", *J. of Soil Mech. and Found. Engineering*, ASCE 1970: 96(5): 1629-1653.
10. **Duncan J. M., Byrne, P, Wong, K., Mabry P.,** "Strength, stress-strain and bulk modulus parameters for finite element analyses of stresses and movements in soil masses", *Report UCB/GT/80-01*, Univ. of California, Berkeley, CA, USA, 1980.
11. **M.C. Nataraja, N. Dhang, A.P. Gupta**, "Stress-strain curves for steel-fiber reinforced concrete under compression", Cement & Concrete Composites, 1999, 21, 383-390.

The Authors

E. Stavrotheodorou, Ph.D. candidate, Dept. of Civil Engineering, University of Thessaly (elenstavrotheodorou@yahoo.gr). She received her MSc in "Applied Mechanics and Systems Modelling and Simulation" in 2008 and her MSc in "Spatial Analysis and Environmental Management" at the University of Thessaly in 2010. She received the first award in a Panhellenic Competition for her Diploma Thesis in 2007. She taught at the Technological Educational Institute, Larissa, Greece, Department of Infrastructure Engineering. She has worked as supervisor engineer on public works projects since 2006.

P. Dakoulas is an Assoc. Professor of Civil Eng. at the Univ. of Thessaly (dakoulas@uth.gr). He received his PhD at RPI, N.Y., in 1985 and taught at Rice University, Houston, Tx, till 2001. His research is in the area of soil dynamics, constitutive modeling and numerical methods. He served as chair of the Earthq. Eng. & Soil Dynamics Committee of ASCE from 1992 to 2000 and as member of the Editorial Board of the J. of Geotechn. and Geoenviron. Engineering. He is the author or co-author of more than 100 journal papers, conference papers and other publications. He received the Prakash Award in 1995 and Hsieh Award of ICE in 2009. He has served as consultant on projects related to earth dams, bridges, gas pipeline systems, offshore foundations, etc.